On the near-wall structure in reverse-flow and post-reattachment recovery regions of separated flow and its equivalence to the structure in wall and free-surface jets

A. Dejoan and M.A. Leschziner

Department of Aeronautics, Imperial College London,

London SW7 1AZ, UK.

Email: a.dejoan@imperial.ac.uk, mike.leschziner@imperial.ac.uk

Abstract

The statistical and structural properties of two wall jets, one developing along a real wall and the other along a shear-free wall, are contrasted with the equivalent properties in the post-reattachment recovery and reverse-flow region of a separated backward-facing step flow, respectively. The study was motivated, principally, by the wish to isolate and understand the mechanisms possibly responsible for the poor representation of the post-reattachment recovery returned by most RANS closures. It demonstrates a substantive commonality in the turbulent processes between, on the one hand, the real wall jet and post-reattachment recovery, and on the other hand, between the frictionless-wall jet and the reattachment zone as well as the reverse-flow near-wall layer

in the backward-facing-step flow. All regions under consideration are found to be characterised by an influential interaction between an outer shear layer and the wall, but an important distinction arises from the presence or absence of strong near-wall shear, which introduces significant changes to the nature of this interaction: in the absence or near-absence of wall shear, the interaction is largely inviscid, associated with wall-blocking, while strong shear tends to shield the wall from the outer flow. The commonality between the two sets of flow conditions is explored by way of mean-flow properties, budgets, anisotropy maps, departures from local equilibrium, non-dimensional strain parameter, length-scale variations and structural properties. The study shows that the post-reattachment recovery, like the real wall, is far from local equilibrium and that the near-wall region is strongly affected by turbulent diffusion associated with the migration of large-scale structures towards the wall. In statistical terms, this is represented by the importance of turbulent transport by third moments and pressure-velocity correlations. The recovery of the flow towards a state equilibrium is slow. Within the reattachment and reverse-flow layer, near-wall shear is weak, and likewise the shielding of the wall from the outer layer. In these regions, the flow shares many of the properties of the zero-wall-shear jet.

1   Introduction

The correct prediction of separation over a broad range of geometric and flow conditions remains a major challenge to even the most advanced tur-

bulence models, at whatever level of closure [1], [2]. Although the overall features and dimensions of recirculation zones are returned correctly by some turbulence models, their detailed features are almost always misrepresented. One common defect which occurs almost invariably, whatever the predictive quality in the recirculation zone itself may be, is an insufficient rate of post-reattachment recovery. The ubiquity of this defect suggests that the problem may lie in the complex interaction between the outer shear layer, originally above the recirculation zone, and the wall over which the wake recovers. The effect of the wall is two-fold: first, it acts to block the wall-normal velocity fluctuations and to reflect pressure fluctuations, thus modifying the turbulence field away from the wall in the shear layer; and second, it causes the formation of a sheared boundary layer, with its own scales and turbulence characteristics, which interacts with the outer shear layer, thus affecting its evolution. Within the recirculation zone itself, the near-wall backward flow may also be regarded as an amalgam of (at least) two disparate shear layers: the outer one originating from the lower part of the post-separation free shear layer, subjected to strong curvature as a consequence of reattachment, and the inner one being the boundary layer originating at the reattachment point line. However, here, the boundary layer is very thin, and the flow is, most likely, dominated by the outer shear layer interacting almost inviscidly with the wall. Both the post-reattachment recovery layer and the reverse-flow layer are highly perturbed, in addition to being composite layers, by the strong curvature and normal straining associated with the impingement process in the reattachment region.

It is the above two-pronged interaction between composite shear layers and the wall that is the focus of the present study. Its principal objective is to gain

insight into the peculiar characteristics of the turbulence processes within the shear layers in the wake recovering from separation and reattachment and in the near-wall layer within the recirculation zone. A second objective is to derive from this insight the implications for modelling recirculating flows, with the emphasis being placed on the recovery zone.

In this context, a flow that appears to be highly pertinent to post-reattachment recovery is the wall jet. This flow also consists of two interacting shear layers, one a separated outer layer and the other a boundary layer. The turbulence processes in this flow have recently been the subject of three studies by the present authors [3], [4], [5], in which data derived from large eddy simulations have been analysed. These studies focus, respectively, on the turbulence structure of the wall jet, on the discrimination of effects arising from wall blocking and wall shear and on a-priori studies of elements of second-moment RANS closures. Some important features that the simulations have brought out include the significant contribution of triple-correlations-driven stress diffusion in the interaction region, the surprisingly high level of pressure diffusion, the strong influence of wall blocking on the redistribution mechanism and the major effects on the turbulence structure brought about by the addition of near-wall shear to wall blocking. An outcome of the a-priori RANS studies [5] has been the illumination of some of the reasons for the poor representation of the above-noted features by popular second-moment-closure models.

The present study contrasts the turbulence characteristics of the recovery and reverse-flow layers of the separated flow behind a backward-facing step against those of two wall jets, one with and the other without wall shear, the comparative analysis being based, principally, on Reynolds-stress budgets and

observations of structural properties. The back-step-flow simulations were undertaken by the present authors in the context of a study on the control of separation by means of a synthetic jet [6] which perturbs the separated shear layer. Here, the data for the unperturbed flow are exploited. The rationale is to identify parallels in the turbulence mechanisms and to understand the extent to which the supposition of the equivalence of the processes in the regions of interest within the recirculating flow and the jets is valid. As will emerge, there are indeed a number of fundamental statistical mechanisms that link the two flows, despite the self-evident differences in their global characteristics.

2 The flow configurations and their simulations

The flow configurations studied are shown in Fig. 1. The back-step flow is at a Reynolds number $Re = U_c h/\nu = 3700$, at conditions identical to those of the experiments of Yoshioka *et al.* [7]. The computational domain extends from $4h$ upstream of the step to $18h$ downstream. The spanwise direction is statistically homogeneous and $4\pi/3$ deep. A two-block grid of 2.10^6 nodes is used, with the maximum ratio of the grid scale, Δ, to the Kolmogorov scale, η, not exceeding 7 throughout the domain, see top Fig. 2. The maximum value of $y^+ = yu_\tau/\nu$ at both the lower and upper walls is less than 1, and the cell-aspect ratio is, typically, $\Delta y^+/\Delta x^+/\Delta z^+ = 1.1/18/10$ at the wall and $2.5/18/10$ in the shear layer. The inlet conditions, prescribed at $4h$ upstream the step, were derived from a fully-developed channel-flow precursor computation carried out over a domain of $2h \times 2\pi h \times 4\pi h$ with

streamwise-periodicity imposed.

The wall jet is at a Reynolds number $Re = U_o b/\nu = 9600$, U_o being the inlet velocity and b the slot height. Two cases were simulated, one in which the jet develops along a real wall and the other along a frictionless, impermeable boundary. Here, the intention is to permit effects arising from wall-blocking and near-wall shear to be distinguished or separated within the whole interaction process between the outer shear layer and the wall. The real jet simulated corresponds to one studied experimentally by Eriksson *et al.* [10]. In both jet flows, the domain extends from the wall to $10b$ above it and to $22b$ in the streamwise direction. The grid is composed of 8.10^6 computational cells, and the ratio Δ/η is typically $5-10$, see Fig. 2. For the real jet, the near-wall cell-aspect ratio is, typically, $\Delta y^+/\Delta x^+/\Delta z^+ = 1.2/24/24$, the wall-nearest grid node located at $y^+ = 0.6$. More details can be found in [3], [4].

Computational tests, including the use of different grid-resolution levels and subgrid-scale models, have shown the back-step-flow simulation to be insensitive to subgrid-scale modelling, and the standard (damped) Smagorinsky model was therefore adopted. A complete description is given in [6]. The transitional character of the wall jet, albeit only within a few slot heights downstream of the discharge, made the use of Germano's dynamic Smagorinsky model more appropriate for this flow, yielding good agreement between the simulation and the experiments (see [3]).

3 Results

3.1 Preliminaries

A few results for mean-flow quantities and second moments are presented first, in order to convey a global view, but the emphasis is on budgets and structural features. For the back-step flow, properties are normalised by the step height h and the maximum velocity in the inlet channel U_c. Results for the jet flows are given only at the far-field location, $x = 20b$, where the flow approaches a state of self-similarity. Here, the flow properties are normalised with the maximum velocity, U_{max}, and $y_{1/2}$, the distance from the wall to the half-of-maximum-velocity point (see Fig. 1). Using this scaling, the outer layers of the two jets display a self-similar behaviour (see [4]).

3.2 The mean flow and the turbulence properties

Figures 3-10 presents profiles of the mean-velocity and Reynolds shear stress for all three flows considered. For the back-step flow, the profiles are given at two locations ahead of the reattachment location ($x_r = 7h$) and one, well downstream, in the recovery region. The data are compared with two sets of experimental results, one by Yoshioka *et al.* [7] and the other by Kasagi *et al.* [11], as well as with the DNS results of Le *et al.* [12], the last two being for a Reynolds number of 5100 – that is, not far above the present value. However, the DNS data relate to a geometry that does not include an upper wall. Considering the differences, the comparisons show fair agreement among the results. An exceptional feature is the high streamwise stress predicted by the present simulation at the upper wall. This reflects the fact that, at the lower Reynolds number pertaining to this simulation, the flow along this wall

is incipiently separated, with separation occurring intermittently. It is also noted that Yoshioka *et al.* report a shorter reattachment length, $x_r = 5.5h$, than the present value of 7, this discrepancy being most likely due to 3D contamination in the experiments, an issue discussed in [6], where also a complete comparison of the full turbulence statistics is included.

A global view of the recovery region is conveyed in Fig. 8 by way of universal velocity profiles at 1.59 and 2.32 times the reattachment distance, x_r. The profiles demonstrate the slow recovery towards an equilibrium state, identified by the log law. The depressed velocity region, with roughly correct log slope, is the region in which the outer shear layer and the inner boundary layer interact, and it will be shown latter that this region is characterised by a slow evolution towards the equilibrium state associated with the effects of the outer layer. The detailed mechanisms contributing to this slow recovery will also be discussed below by reference to the budgets and structural features.

For the real wall jet, extensive comparisons with the experiments are presented and discussed in [3], while a detailed discussion on the discrimination of wall-blocking effects from wall-shear effects is given in [4]. Here, profiles of mean velocity and Reynolds stresses in the (nearly) self-similar region are included in Figs. 9 and 10, respectively, to highlight some major differences between the two jets. Such differences between the two wall jets arise from the non-vanishing values of the streamwise and wall-parallel stresses at the wall of the wall-shear-free jet. In the absence of wall-shear, large eddies originating from the outer layer *impinge* on the wall without damping by viscous action, thus resulting in a high finite value of turbulence energy at the wall. The near-wall structural features of the two jets also differ greatly. In particular, the near-wall shear gives rise to small-scale, elongated eddies, while in

the absence of shear, the eddies are more "isotropic". This implies different redistribution mechanisms of turbulence energy among the normal stresses in the near-wall region, discussed in more detail in [4].

3.3 Budgets

The selection of budgets included herein are intended to highlight features common to both wall jets and the back-step flow. For the former, budgets are reported for $x/b = 20$, where the flow is close to being self-similar. For the latter, they are given for two locations, one at $x/h = 7$, close to the mean reattachment location, and the other well downstream of the reattachment point, at $x/h = 16$. The budgets at $x/h \leq 7$ were found to be very similar to the corresponding ones at other locations within the recirculation zone and, indeed, around the time-averaged reattachment location. This is illustrated by the comparison, in Fig 11, between the turbulence-energy budgets $x/h = 7$ and $x/h = 4$, which are seen to be closely similar. The preferential focus on the location $x/h = 7$ is motivated by the fact that at this location the wall-shear vanishes, a state corresponding to the free-shear jet. The terms included in the budgets terms are those constituting the transport equations that govern the evolution of the stresses:

$$
\frac{\partial \overline{u_i u_j}}{\partial t} + \underbrace{\overline{U}_k \overline{u_i u_j}_{,k}}_{C_{ij}} = \underbrace{-\overline{u_k u_j} U_{i,k} - \overline{u_k u_i} \overline{U}_{j,k}}_{P_{ij}}
$$
$$
+ \underbrace{\nu \overline{u_i u_j}_{,kk}}_{D_\nu} \underbrace{-\overline{u_i u_j u_k}_{,k}}_{TTT_{ij}} \underbrace{- \frac{(\overline{u_i p_{,j}} + \overline{u_j p_{,i}})}{\rho}}_{\Pi_{ij}} \quad (1)
$$
$$
+ \underbrace{\varepsilon_{ij}}_{\text{dissipation}}
$$

9

The turbulence-energy budget is deduced from the sum of the normal-stress equations. Here, we point out that the dissipation is deduced from the balance of Eq. (1), which implies that ε_{ij} represents the total level of dissipation, including the viscous and subgrid-scale contributions. While the latter also contains non-dissipative fragments, the contribution is insignificant. Indeed, the level of the subgrid-scale term as a whole is rather low in the present simulations. Thus, typically, the level of dissipation rate of the turbulence energy, evaluated from the exact definition, was found to be of order 50-70% of that determined from the imbalance, and both were observed to have very similar qualitative features.

The budgets for the turbulence energy are shown in Fig. 11. The main feature linking the reverse-flow ($x/h = 4$) and reattachment regions of the backward-facing step ($x/h = 7$) to the zero-wall-shear jet is the low near-wall shear production. At the reattachment, production is close to zero. With the near-wall shear being very small, it is observed that the main input of turbulence energy into the near-wall layer is caused by a high level of turbulent transport from the outer shear layer towards the wall, in particular in the respective interaction layers $0.05 < y/h < 0.25$ and $0.02 < y/y_{1/2} < 0.2$, although convection is also significant, because of the slip at the wall in the zero-wall-shear jet. Very near the wall, both energy budgets indicate a balance mainly between turbulent transport (combining triple correlation and pressure diffusion) and dissipation.

Downstream of reattachment, as the flow recovers, a new boundary layer develops, and mean-shear production close to the wall becomes a major contributor to the turbulence energy. Here, a balance qualitatively akin to that in a standard boundary layer is observed, wherein production is mainly bal-

anced by dissipation in the near-wall region. However, a major difference to a standard boundary layer is the large input of energy by turbulent transport from the outer shear layer towards the wall, in particular in the interaction region ($0.15 < y/h < 0.3$). While in the reverse-flow zone, the turbulent transport provides the main input of energy, this process contributes equally with production in the interaction region of the recovery region. This combined influence is also observed in the wall jet, although the contribution of diffusion is more pronounced as the production is low in the interaction region ($0.08 < y/y_{1/2} < 0.25$).

Distributions of production-to-dissipation ratio and integral length-scales, given in Figs. 26-25, respectively, will be discussed later in some detail. However, it is useful to highlight here that these distributions demonstrate that the high input of turbulent transport from the outer shear layer towards the wall, in both the wall jet and the recovery region, results in strong departures from equilibrium in the interaction regions – stronger in the wall jet than in the back-step flow, because production is lower in the former than in the latter. Nevertheless, it is this process that is mainly responsible for the strong departures from the log law, observed earlier in Fig. 8.

Budgets for the shear stress are presented in Fig. 12. All show significant levels of transport by triple correlations in the near-wall region. However, in the back-step flow, this transport is negative, while it is positive in both jet flows, this difference being associated with the opposite signs in the respective strain rates (see Figs. 3-9). Both in the recirculation region of the back-step flow and in the zero-wall-shear jet, the production is low, and the main balance occurs between turbulent transport and pressure-velocity correlation. On the other hand, in the back-step recovery region and in the real wall jet,

production is high, and this is counterbalanced mainly by pressure-velocity correlation. However, the contribution of transport by triple correlations is still significant.

Of the normal-stress budgets, those for the wall-normal component are the most interesting and informative, because the wall-normal intensity is intimately linked to the shear stress. On the whole, the budgets of $\overline{uu}$ are similar to those of the turbulence energy, and the budgets of $\overline{ww}$ do not differ greatly among the three flows examined herein, all being broadly similar to those found in a standard boundary layer.

Figures 13 shows that the budgets for the back-step flow within the separation region and in the recovering wake have features similar to those of the zero-wall-shear and the real wall jet, respectively. Thus, the pair of budgets on the left-hand side of Fig. 13 both feature a high level of transport by triple correlations from the outer layer towards the wall, which is compensated by a high negative contribution of the pressure-velocity correlation in the near-wall region, this latter contribution being, in absolute terms, higher than dissipation. However, in the back-step flow, dissipation tends to become more important as the flow recovers. As regards the budget for real wall jet, the stress $\overline{vv}$ is also elevated by a large gain through turbulent transport, but a lower and slightly negative pressure-velocity correlation arises near the wall, the dissipation being here the dominant process. It is important to point out that the $\overline{vv}$ budgets for both the back-step flow in the recovery region and the real wall jet differ strongly from that for the standard boundary layer, in which turbulent transport is low, the main balance being between a large gain by pressure-velocity correlation and loss by dissipation in the near-wall region. This implies that the large gain of turbulent transport modifies the

12

energy-redistribution process in the present wall flows, when compared to a standard boundary layer. Further details will be given below by reference the non-deviatoric part of the velocity-pressure correlation. It is finally noted here that Kuroda *et al.*[13] also reported a prominence of turbulent transport in the budgets of the Reynolds stresses in their DNS of a channel in which the wall-shear stress on one wall is much lower that that on the other wall, resulting in a turbulent Couette-Poiseuille flow. Turbulent transport is even more pronounced in the present flow, because of the presence of the outer shear layer.

3.4   The near-wall flow structure

The budgets presented in the previous section above brought to light some significant similarities between the processes in two disparate regions in the backstep flow and those in the two wall jets examined. As shown in the present section, these similarities may be associated with corresponding structural features in the wall region of the two juxtaposed flows.

The instantaneous contours of the streamwise-velocity fluctuations represented on Fig. 14 suggest a very different wall structure between the reverse-flow region and the recovery region of the backstep flow. As the flow recovers, the near-wall structure, here visualized by way of contours of streamwise-velocity fluctuations is dominated by "streaky", fine and elongated features, which are characteristic of alternate high- and low-speed streamwise fluctuations. In contrast, in the reverse-flow region, close to the nominal reattachment location, the contours indicate a far more "isotropic" structure. Figure 15 shows that the corresponding near-wall structure of the zero-wall-shear jet is, likewise, characterised by rounded rather than streaky features. This

commonality reflects the fact that in both flows the dominant near-wall mechanism is the "splatting" of eddies originating from the outer flow, onto the wall without preferential wall-parallel orientation. For the wall jet, the details of the process are discussed extensively in [8]. Here, they are illustrated by instantaneous fields of contours of the velocity-fluctuation vector $(v/U_o, w/Uo)$ depicted in the upper plot of Fig. 16 across a wall-normal (y, z) plane just upstream the reattachment location, in comparison with a corresponding upper plot in Fig. 17 for the self-similar region of the zero-wall-shear jet. Both fields exhibit a pattern that indicates large-scale eddies originating from the outer layer, migrating towards the wall and then impinging upon it. In the case of the zero-wall-shear jet, viscous effects are negligible, and the intensity of "splatting" is high. In the back-step flow, on the other hand, the imposition of zero slip at the wall introduces some measure of viscous damping, but the dominance of splatting is nevertheless evident, and impinging motions of large eddies originating from the outer layer penetrate up to the wall, as is evident from the upper plot in Fig. 16.

Downstream of reattachment, the flow recovers, and the wall shear increases progressively. Thus, here, the strained near-wall layer partially insulates the wall from splatting, and the near-wall layer is characterized by a streaky structure with splatting damped, as seen from Figs. 14 and 16 (lower plots). Similar characteristics are observed in the real wall jet, as shown in the lower plot of Fig. 17).

Specifically in respect of the streaky layer, it is interesting to refer here to DNS studies by Lam and Banarjee [9] who have shown that the formation of streaks is not tied primarily to the presence of the physical wall itself, but is a consequence of high shear. In their numerical experiments they imposed

a mean shear onto a free-slip surface and observed the formation of streak for sufficiently high shear even without a wall. At low shear, however, no streaks form in the surface layer or near a wall. Lam and Banarjee further identify the nondimensional strain, $\tilde{S} = \frac{\overline{uv}S}{\varepsilon}$ ($S = \frac{\partial U}{\partial y}$) as the parameter governing the formation of streaks. They show that streaks can form when $\tilde{S} \geq 1$, and that, the higher the parameter $\tilde{S}$ is, the more pronounced are the streaks. To investigate this dependence, Fig. 18 presents several profiles of $\tilde{S}$, namely three from the present backstep-flow simulations, at $x/h = 4, 10$ and 15, two from Le et als et $al.$ DNS for a similar backstep flow, at $x/h = 10$ and 19, and two profiles (from the present computations and the DNS) in the channel upstream of the step, in which the flow is fully-developed. Inside the recirculation region, at the location $x/h = 4$, the parameter has a negative value because of the shear stress and shear strain are de-correlated through the strong effects of other strains on the shear stress. The negative turbulence-energy production in this region (see Fig. 11) is also a reflection of this de-correlation. However, the magnitude of $\tilde{S}$, arguable the appropriate quantity to consider, is well below 1, which is compatible and consistent with the absence of streaks in this region (see top plot in Fig. 14). Following reattachment and recovering over approximately 3 step heights, the peak $\tilde{S}$, associated with the maximum mean shear production, rises towards and exceeds 1, and this leads to the formation of the streaky structure at around $x/h \geq 10$, as shown in Fig. 14. However, comparison with the channel-flow variations shows that $\tilde{S}$ rises only slowly, and that its value at $x/h = 15$ is still considerably smaller than the level in the channel flow. Indeed, in the DNS of Le et al, $\tilde{S}$ hardly rises at all between x/h=15 and 19. This is, again, a facet of the slow recovery of the post-reattachment flow and the response of

15

the near-wall layer to shear in the presence of the influence of the outer layer. The maximum value $\tilde{S} > 2$ is found to arise in the wall jet, and this higher value is indeed associated with a more pronounced streaky wall structure, as illustrated by the contrasting structures in the lower plots in Figs. 14 and Fig. 15. For this flow, the present authors (see [8]) have shown that the thin wall layer, where the streaks form, is robust and acts as a "shield" which protects the wall itself from the large eddies impinging upon it. This feature was shown to be instrumental in the damping of the fluctuations as the wall is approached, and to result in a redistribution process of turbulence energy very different from the zero-wall-shear jet.

In the following section, the wall-limit behaviour of the turbulent fields is discussed by reference to the level of near-wall anisotropy and the redistribution of turbulence energy among the normal stresses through the pressure strain process.

3.5   Redistribution of energy and anisotropy

Scalar measures indicative of the level of the anisotropy are the second and third anisotropy invariants, $II = b_{ij}b_{ij}$ and $III = b_{ij}b_{jk}b_{kj}$, respectively, in which $b_{ij} = \overline{u_i u_j}/k - 2/3\delta_{ij}$ is the anisotropy tensor (see Fig. 19). A third interesting invariant, derived from those above, is Lumley's flatness parameter $A = 1 - 9/8(II - III)$. This parameter varies between the limits of 0, indicating two-component turbulence (at a wall or sharp interface) and 1, indicating isotropy. The variation of this parameter is especially pertinent in the context of turbulence modelling, as it is often used to procure the appropriate sensitivity of the pressure-strain approximation and dissipation equation to the proximity of the wall.

16

Prior to an examination of the above invariants, it is instructive to consider the normal components of the anisotropy tensor, b_{ii}, and this is done in Fig. 19. A point to note first is that the main distinction between the two wall jets relates to b_{11} and b_{33}. In both cases (indeed, at any wall), b_{22} must approach -1/3, as the wall-normal intensity vanishes. In the wall-shear-free jet, the wall-parallel anisotropy components at the wall are very similar; it is only away from the wall where b_{11} is substantially higher due to wall-shear production. When wall is introduced, b_{11} rises steeply close to the wall, and b_{33} drops correspondingly, suggesting substantially different energy-redistribution processes in the two flows. Corresponding differences are seen when comparing the distributions of the anisotropy components in the two regions of interest in the backstep flow. Around and ahead of the reattachment point, b_{11} and b_{33} are similar close to the wall. As wall shear becomes influential in the recovery region, these same components diverge in the same manner as they do in the wall jets. These common features are reflected by corresponding similarities in the behaviour of A considered next.

Fig. 20 contrasts profiles of A for the backstep flow at 4 locations against those derived for the two wall jets. As expected, all profiles asymptote to zero at the wall, indicating the approach to the two-component limit. In both the wall-shear-free jet and upstream of the reattachment location in the backstep flow, A remains high close to the wall, and then drops steeply towards zero. This suggests a deeper penetration of the large eddies towards the wall when wall shear is low. In contrast, as the backstep flow recovers, the near-wall anisotropy increases, due to the increasing level of shear-induced production, and the penetration of large structures from the outer flow decreases significantly. This feature is also observed when wall shear is introduced to the wall

jet. It is also interesting to compare the profiles of A in the recovery region of the backstep flow with those for the channel flow and the self-similar region of the real wall jet, and this is done in Fig. 21 in terms of wall scaling (note that no such comparison is possible for the shear-free wall jet, and this the reason for using outer scaling in the previous figure). These profiles bring to light the high near-wall anisotropy of the wall jet, relative to the recovery region, and this is consistent with the higher level of $\tilde{S}$ in the wall jet, seen in Fig. 18 and indicating high strain and high shear production. As noted earlier, the high value of $\tilde{S}$ for the wall jet goes hand-in-hand with the presence of a robust streaky structure in the wall region of this flow, protecting the wall from splatting. In the recovery region of the backstep, $\tilde{S}$ is considerably lower, and the streaky near-wall layer is less resistant to the penetration of the impinging motions from the outer layer when compared to the real wall jet. This observation provides, on the one hand, some insight into the mechanisms inhibiting recovery towards equilibrium, and is consistent, on the other hand, with the high negative near-wall peak of the velocity-pressure correlation of the normal stress $\overline{vv}$, needed to balance the high input of turbulent transport in the absence of strong near-wall shear. Thus, the relatively low level of $\tilde{S}$ inhibits the near-wall damping of velocity fluctuations, leading to higher level of near-wall flatness parameter and more vigorous near-wall motions and pressure fluctuations.

One encouraging observation emerging from Fig. 24 and Fig. 20 is that A is well correlated with the wall-normal, non-deviatoric pressure-velocity correlation, Φ_{vv}, regardless of whether or not the near-wall flow is sheared. Thus, A appears to be a good indicator of the damping imparted to the wall-normal stress. On the other hand, the very different behaviour of Φ_{ij} (and

18

also the anisotropy of the dissipation) calls into question the usefulness of A as the only parameter representing the effect of wall proximity in models for Φ_{ij} and ε_{ij}.

A more differentiated view of the anisotropy than that conveyed by A is provided by so-called anisotropy maps, which co-relate the second and third anisotropy invariants, II and III, respectively. Such maps are included in Figs. 22 and 23. Lumley has shown that any realisable state within any turbulent flow must fall within the triangular region. The loci shown within the realisability maps identify traverses across the flows in question, starting from the lower wall and progressing upwards in the direction of the arrows along the loci. Free shear layers are known to exhibit loci that are broadly aligned with the lower, left-hand line of the triangular domain, characterising "axisymmetric expansion". This is a behaviour returned by the zero-wall-shear jet and also by the lower near-wall layer of the backstep flow at $x/h = 7$ (as well as at $x/h = 4$, not included here). At the wall, turbulence tend to a two-component state (as $\overline{vv}$ declines rapidly). This state is identified by the upper side of the triangle. In the presence of wall shear, there is a tendency for II and III to move upwards, broadly parallel to the lower right-hand line of the triangle. This is a behaviour characteristic of near-wall shear. In fact, in a conventional boundary layer, the state of anisotropy in the log-law region is characterised by a locus hugging the lower right-hand-side line. The real wall jet features a thin near-wall region that is akin to a log-law layer. However, the mean-velocity profile for the wall jet, reported in Dejoan and Leschziner [3], shows that this log layer is thin and indistinct, reflecting the strong influence of the outer shear layer on the near-wall region. A qualitatively similar behaviour is observed in the lower near-wall layer of

19

the backstep flow at x/h=15. Again, there is a tendency for the locus to rise, but clearly the anisotropy state in this layer is far from that of an equilibrium layer (or indeed the upper-wall layer).

A process that plays a particularly important role in relation to anisotropy is the pressure-velocity interaction Π_{ij}. This term is conventionally split into two fragments, $\Pi_{ij} = \Phi_{ij} + d_{ij}$, where $\Phi_{ij} = \overline{\frac{p}{\rho}(u_{i,j} + u_{j,i})}$ corresponds to the pressure-strain term and $d_{ij} = -\overline{\frac{1}{\rho}(u_i\delta_{kj} + u_j\delta_{ki})}_{,k}$, to the pressure diffusion term. The pressure-strain term, Φ_{ij}, is trace-free and thus responsible for the redistribution of the energy among the normal-stress components. This term is not only highly influential, but one that presents major challenges to closure at second-moment level. It is therefore of considerable interest.

Against this background, Figure 24 shows profiles of the pressure-strain components relating to the normal stresses. One particularly interesting feature, linking the present considerations to the earlier discussion of b_{ij}, is the similarity of the energy-redistribution processes in the recirculation region and the zero-wall-shear jet. In both cases, this redistribution is from $\overline{vv}$ to both $\overline{uu}$ and $\overline{ww}$. As the separated flow recovers, the energy-redistribution process becomes similar to the real wall jet, wherein the energy is transferred from $\overline{vv}$ and from $\overline{uu}$ to $\overline{ww}$. Again, this links well with the previous observations on the behaviour of b_{ij}. In the latter case, a high level of $\overline{uu}$ is produced by the near-wall shear, and energy has to be removed from $\overline{uu}$, so that all stresses are made to vanish at the wall (see [4] for more details). A point of difference between the wall jet and the recovery region lies in the near-wall variation of Φ_{uu}. Specifically, this components features a distinct negative peak wall jet in the case of the wall jet, while this feature is absent in the recovery region of the backstep flow. This is likely to be linked to

corresponding differences in the level of $\tilde{S}$ which is significantly higher in the wall jet, thus resulting in higher generation that needs to be compensated by an elevation of Φ_{uu}.

These similarities highlighted above suggest strongly that wall-blocking effects dominate over the wall-shear effects inside the recirculation region of the back-step flow. In contrast, as the flow recovers, wall-shear effects exert a much greater influence, although the effects are not as strong as observed in the wall jet. As demonstrated by the present authors for the wall jets [4], the energy-redistribution is closely linked to structural features near the wall – in particular, the "splatting" of large-scale eddies onto the wall and the shielding and damping effected by the near-wall shear layer.

3.6   Length scale and equilibrium

It is of interest to examine the near-wall variation of the integral length scale $k^{3/2}/\varepsilon$, normalised by the equilibrium length scale $C_\mu^{-3/4}\kappa y$, as these indicate, alongside variations of the production-to-dissipation ratio, P/ε, departures from local equilibrium. Such profiles are given on Fig. 25. In the back-step flow, as the outer layer develops, the length scale increases in the wall region of the recirculation zone. In the reattachment region, $x/h = 7$, where the outer layer interacts especially strongly with the wall, the length scale close to the wall reaches a maximum value and then diminishes as the flow recovers and a near-wall layer forms. A high value for the integral length scale is also observed in the zero-wall-shear jet relative to the real wall jet, and this reflects the presence of intense, large-scale outer-layer motions towards the wall, which are not damped by viscous and shear-induced effects. Very close to the wall, the steep rise in the normalised length scale is, for this flow,

21

rather misleading, because the length scale itself remains finite at zero shear, while y declines to zero. In the case of the backstep flow at $x/h = 7$, the length scale vanishes at the wall, but is nevertheless substantially elevated in this region relative to the level downstream, suggesting a material influence of the outer layer in this region, similar to that observed in the zero-wall-shear jet. As the flow recovers, shear and viscous effects become influential and tend to reduce the integral length scale, with the near-wall eddies changing their structure to become elongated and smaller in size. However even at $x/h = 15$, the normalised near-wall length scale is substantially above unity, and this suggests that outer-layer turbulence continues to significantly affect the boundary layer in the recovery region. Previous studies (see Hassan, [14]) have indeed reported that the large scale structures issuing from the outer layer tend to persist further downstream reattachment.

As seen in Fig. 25, the length scale within the reverse-flow layer, at $x/h = 4$, is substantially lower than that $x/h = 7$ and also 15. This is rather surprising, at first sight, because all previous comparisons and considerations demonstrated a high degree of commonality between the conditions at $x/h = 7$ and 4 (and thus also with the zero-wall-shear jet). It is recalled, in particular, that the two locations share a low value of near-wall $\tilde{S}$, which signifies the absence of a streaky near-wall layer that shields the wall from the outer scales. In the case of the reverse-flow region, the shear layer above the thin backward-moving boundary layer has a highly complex structure, as a consequence of impingement, strong curvature and recirculation. This is signified, for example, by the negative turbulence-energy production and negative $\tilde{S}$ in this region. Hence, it is difficult to fully interpret the interaction between the outer layer and the near-wall region within the recirculation

zone. The fact that the length scale is rather low in this region must be linked to the negative production, which tends to lower k and hence l_ϵ. The near-wall peak, at around y/h=0.05, does evidently signify that turbulence is transported from the outer layer towards the near-wall region. However, these turbulent motions are less intense inside the recirculation zone than at reattachment because as the vortical structures developing from separation increase in size, their interaction with the wall is intensified and results into high "splatting" events as they reach the wall. Thus, although it might appear that the flow at this position is closer to equilibrium than the two others, the reserve is, in fact, the case, as is well brought out by the distributions of the production-to-dissipation ratio shown in Fig. 26. These distributions demonstrate strong departures from local equilibrium in both the recirculation and impingement regions and immediately downstream of it, due to a combination of low (or negative) production and gain by turbulent transport. A similar behaviour, for identical reasons, is displayed by the zero-wall-shear jet. As the back-step flow recovers, the near-wall peak of the ratio P/ε increases and eventually exceeds unity. Thus here, the near-wall flow does not appear to be far from a state of equilibrium. However, as shown earlier by reference to the parameter $\tilde{S}$ (which in the near-wall region is equivalent to the ratio P/ε, see section 3.4), recovery is actually very slow, and at the farthest downstream location included in the simulation, the near-wall region has not reached the level of anisotropy equivalent to that of a fully developed channel flow. A partial explanation for this apparent inconsistency is provided by the budget of turbulence energy, Fig. 14. For $x/h = 16$, it is observed that convection and diffusion largely compensate each other, so that an approximate balance between production and dissipation is returned above the viscous sublayer.

In the interaction region of the real jet, it is the vanishing shear production, associated with a reversal in the shear strain, that leads to the much lower level of the production-to-dissipation ratio relative to that observed in the recovery region of the backstep flow.

4 Conclusions

The present study has demonstrated, mainly by reference to budgets, anisotropy parameters and near-wall structural properties, that turbulence mechanisms effective in different regions of a separated flow relate to those in two wall jets, one evolving along a real wall and the other along a slip boundary. The latter jet only includes wall-blocking effects in its near-wall region, while the former combines wall-blocking with near-wall shear effects. An interesting finding is the similarity between the wall regions in the impingement and recirculation zone of the back-step flow and the zero-wall-shear jet, which suggests a predominance of wall-blocking effects inside the recirculation zone. In this region, mean-shear production is low, and the main contributor is transport by triple correlations from the free shear layer towards the wall, which is counterbalanced by the pressure-velocity-correlation terms. In the near-wall layer of the back-step recovery region, mean-shear production becomes predominant, and the budgets for the back-step flow contain features that are close those in the corresponding budgets of the wall jet. In particular, transport by triple correlation transport is also important, especially in the interaction region. In fact, in all flow regions considered herein, the turbulent transport provides a significant, if not major, input of energy in the wall-normal stress, a process that is compensated by pressure-velocity corre-

24

lation and dissipation. This type of interaction differs substantially from that in standard near-wall flows close to equilibrium, for which the wall-normal stress is mainly governed by pressure-velocity correlation and dissipation, the transport by triple correlation being small. The redistribution of the turbulence energy among the normal stresses through the pressure-strain process reinforces the similarities between, on the one hand, the reverse-flow layer and the zero-wall-shear jet, in which energy is transferred from the wall-normal component to the both wall-parallel components, and, on the other hand, between the post-recovery region and the real jet, in which shear-produced energy has to be removed from the streamwise-stress component to the spanwise component. The above different energy-redistribution scenarios, applicable to the recirculation and the post-reattachment-recovery regions of the back-step flow, suggest that the importance of wall-blocking effects depends strongly on the streamwise evolution and local structure of the flow, a fact that presents a significant challenge to statistical closures, second-moment models in particular.

The correspondence in the statistical properties identified for the respective flows examined herein have been found to go hand-in-hand with close similarities in structural features in the respective near-wall layers. In the presence of strong shear, a streaky structure arises, while weak or no shear leads to more "isotropic" structure. The former is associated with the formation of a shear layer that shield the wall from large eddies that migrate towards or impinge onto the wall the process that predominates in weak shear. The nondimensional parameter, $\tilde{S} = \frac{\overline{uv}S}{\varepsilon}$, shown to characterise the effects of shear on the near-wall structure in previous sutides related to fully developed flows, also appears to govern the formation of near-wall streaks

in the present flows. For values well below unity, no streaky structure arises, and this has been shown to be so in the zero-wall-shear jet and in the recirculation zone of the backstep flow. On the other hand, values above unity arise in the real wall and in the recovery region of the backstep flow, and in both cases, the near-wall structure is distinctly streaky. The connection between the wall structure and the wall-blocking/near-wall-shear effects presented here suggests that the parameter $\tilde{S}$ can also be viewed as a good indicator of the type of redistribution energy occuring in bounded sheared flows.

Acknowledgements

References

[1] Jang Y-J., Leschziner M. A., Abe K. and Temmerman L., 2002, Investigation of anisotropy-resolving turbulence models by reference to highly-resolved LES data for separated flow. *Flow, Turbulence and Combustion,* **69**, 161–203

[2] Wang C., Jang Y-J. and Leschziner M. A., 2004, Modelling two- and three-dimensional separation from curved surfaces with anisotropy-resolving turbulence closures. *Int. J. Heafit and Fluid Flow,* **25**, 499–512

[3] Dejoan A. and Leschziner M. A., 2005, Large eddy simulation of a plane turbulent wall jet. *Phys. Fluids,* **17(2)**, 025102

[4] Dejoan A. and Leschziner M. A., 2005, Separating the effects of wall-blocking and near-wall shear in the interaction between the wall and the free-shear layer in a wall jet. TSFP 4, Williamsburg, VA USA, June 27–29, Proc. **2**, 401–406

[5] Dejoan A. and Leschziner M. A., 2005, Assessment of turbulence models for predicting the interaction region in a wall jet by reference to LES solution and budgets. Proc. ETMM6, Sardinia, May 23–25, Proc. 97–106

[6] Dejoan A. and Leschziner M. A., 2004, Large eddy simulation of periodically perturbed separated flow over a backward-facing step. *Int. J. Heat and Fluid Flow,* **25**, 581–592

[7] Yoshioka S., Obi S. and Masuda S., 2001, Turbulence statistics of periodically perturbed separated flow over a backward-facing step. *Int. J. Heat and Fluid Flow,* **22**, 393–401

[8] Dejoan A. and Leschziner M. A., 2005, Separating the effects of wall-blocking and near-wall shear in the interaction between the wall and the free-shear layer in a wall jet. Paper submitted to Phys. Fluids

[9] Lam k. and Banarjee K., 1992, On the condition of streak formation in bounded turbulent flow. *Phys. Fluids,* **A** **4**(2), 306–320

[10] Eriksson J. G., Karlsson R. I. and Persson J., 1998, An experimental study of a two-dimensional plane turbulent wall jet. *Expt. in Fluids,* **25**, 50–60

[11] Kasagi N. and Matsunaga A., 1995, Three-dimensional particle-tracking velocimetry measurement of turbulence statistics and energy budget in a backward-facing step flow. *Int. J. Heat and Fluid Flow,* **16**, 477–485

[12] Le H., Moin P. and Kim J., 1997, Direct simulation of turbulent flow over a backward-facing step flow. *J. Fluid Mech.,* **342**, 119–139

[13] Kuroda A., Kasagi N. and Hirata M., 1993, Direct numerical simulation of turbulent plane Couette-Poiseuille flows: effect of mean shear on the near wall turbulence structures. Ninth Symposium on "Turbulent shear flows", Kioto, Japan, August 16-18, **8**, 4-1–4-6

[14] Hassan M. A. Z., 1992, The flow over a backward-facing step under controlled perturbation: laminar separation. *J. Fluid Mech.,* **238**, 73–96

List of Figures

Figure 1: The flow configurations

Figure 2: Ratio of the cell size to the Kolmogorov scale along various grid lines
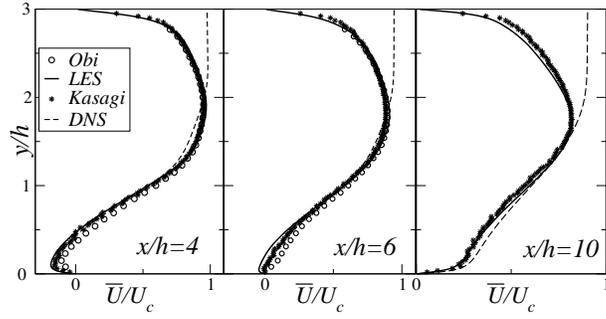
Figure 3: Backward-facing step: profiles of the streamwise-velocity
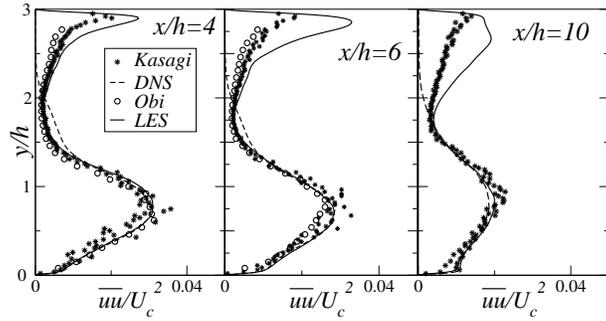
Figure 4: Backward-facing step: profiles of the streamwise Reynolds stress
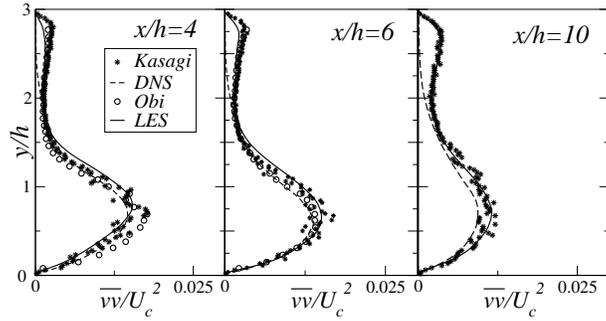
Figure 5: Backward-facing step: profiles of the wall-normal Reynolds stress

33
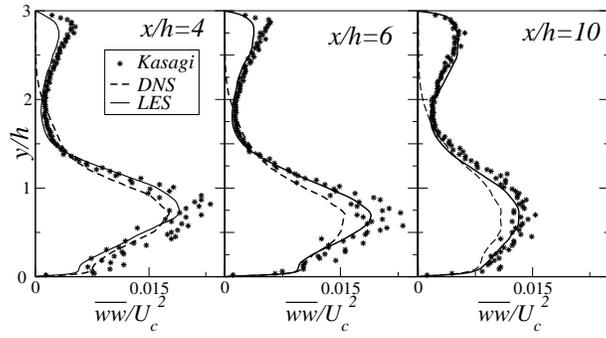
Figure 6: Backward-facing step: profiles of the spanwise Reynolds stress
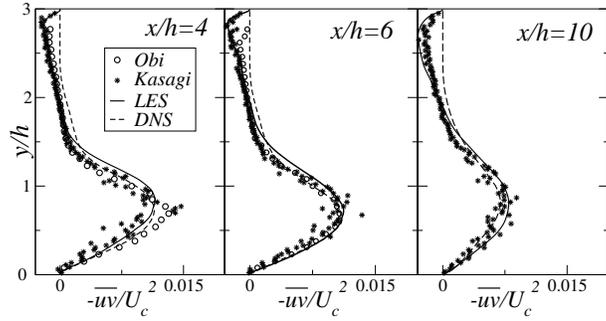
Figure 7: Backward-facing step: profiles of the Reynolds shear stress
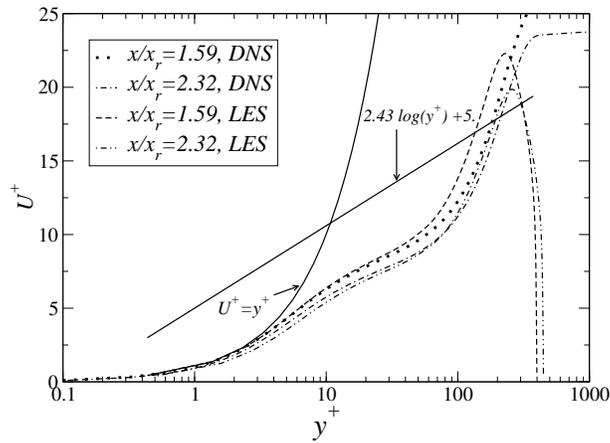
Figure 8: Backward-facing step: log law profiles of the streamwise velocity
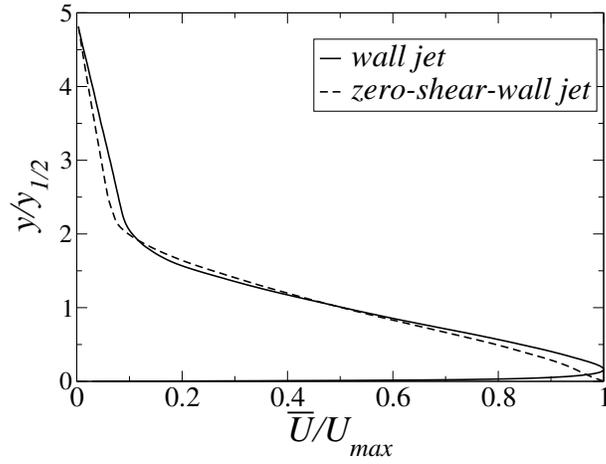
Figure 9: Wall and zero wall-shear jets: profiles of the streamwise-velocity
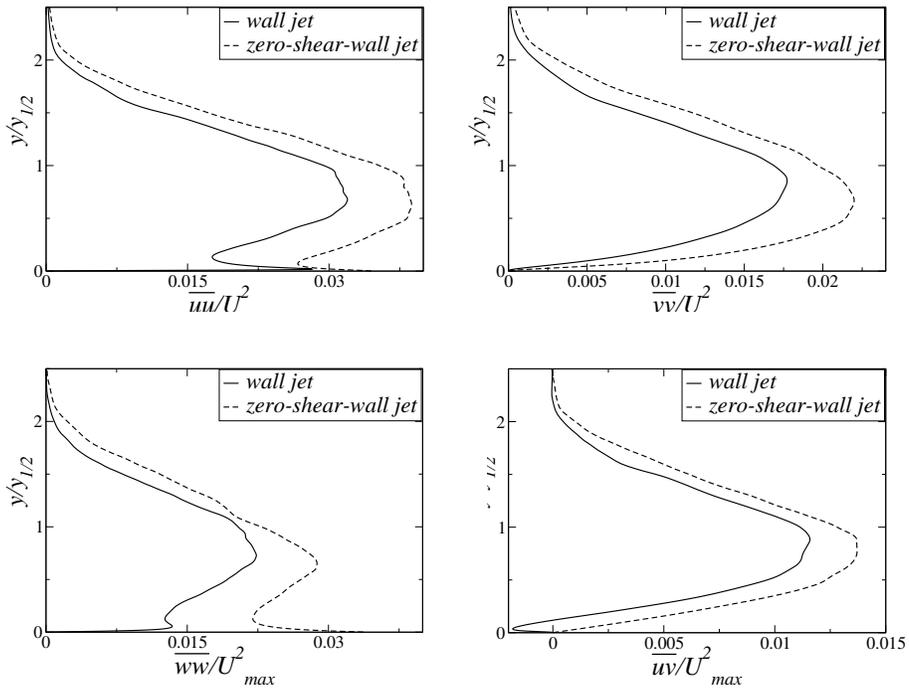
Figure 10: Wall and zero wall-shear jets: profiles of the Reynolds stresses

35
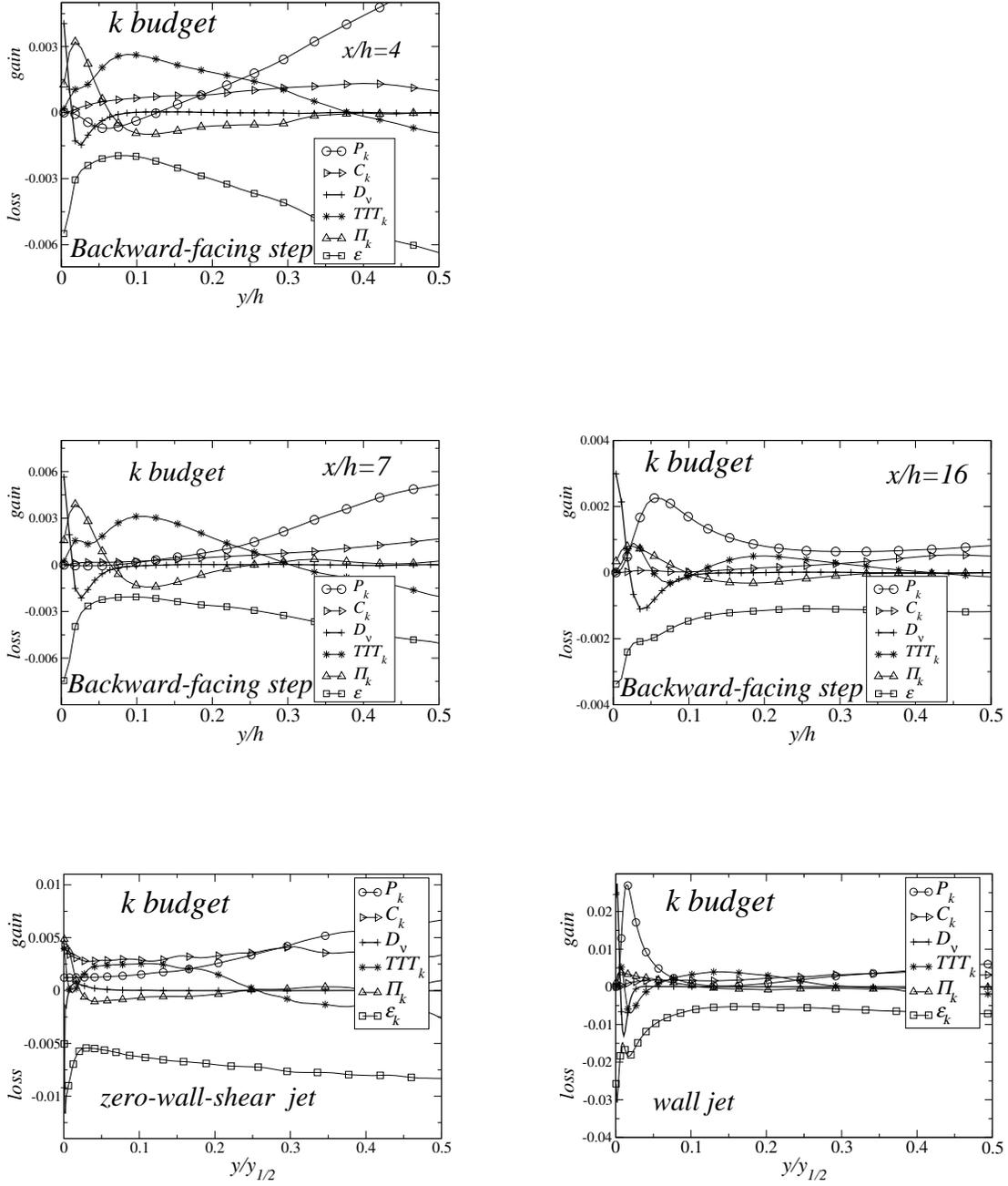
Figure 11: Budgets for the turbulence energy : P: production; C: convection; D_ν: viscous diffusion; TTT: transport by Triple correlations; Π: velocity-pressure correlations (identical to pressure diffusion for k); ε: dissipation. See Eq. (1) for definition of budget terms
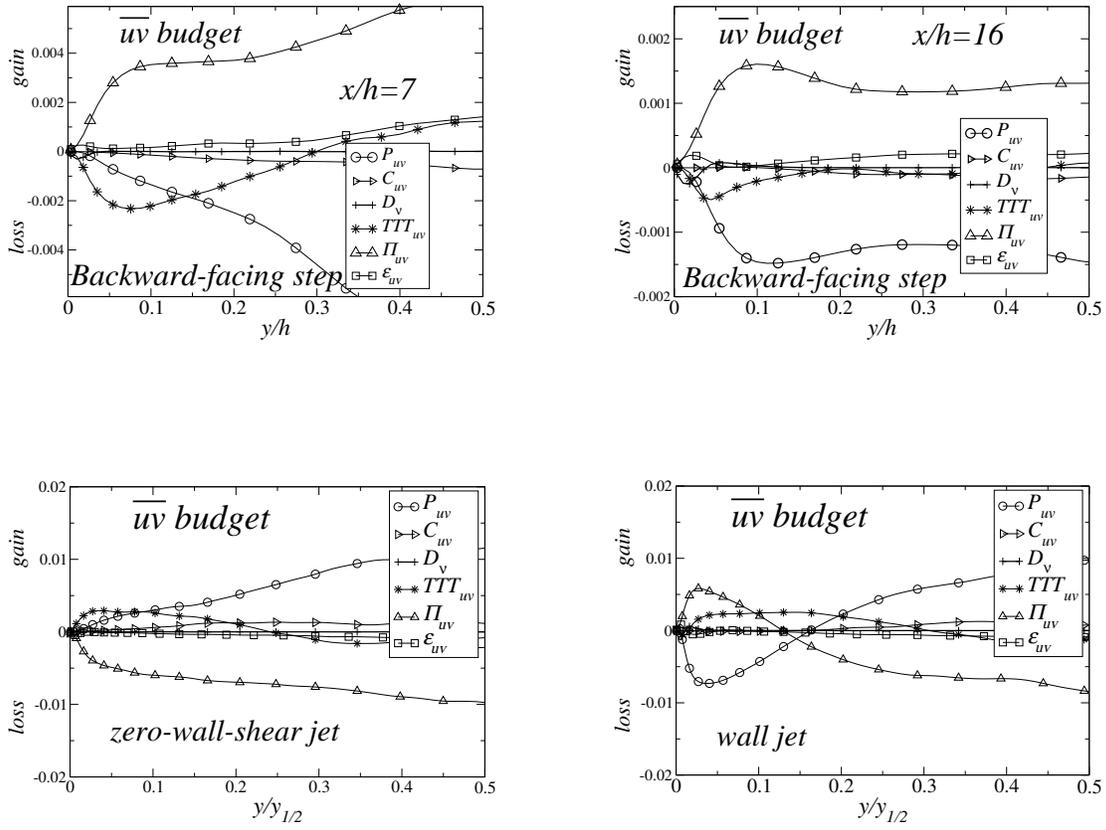
Figure 12: Budgets of the shear stress: see caption of Fig. 11 and Eq. 1
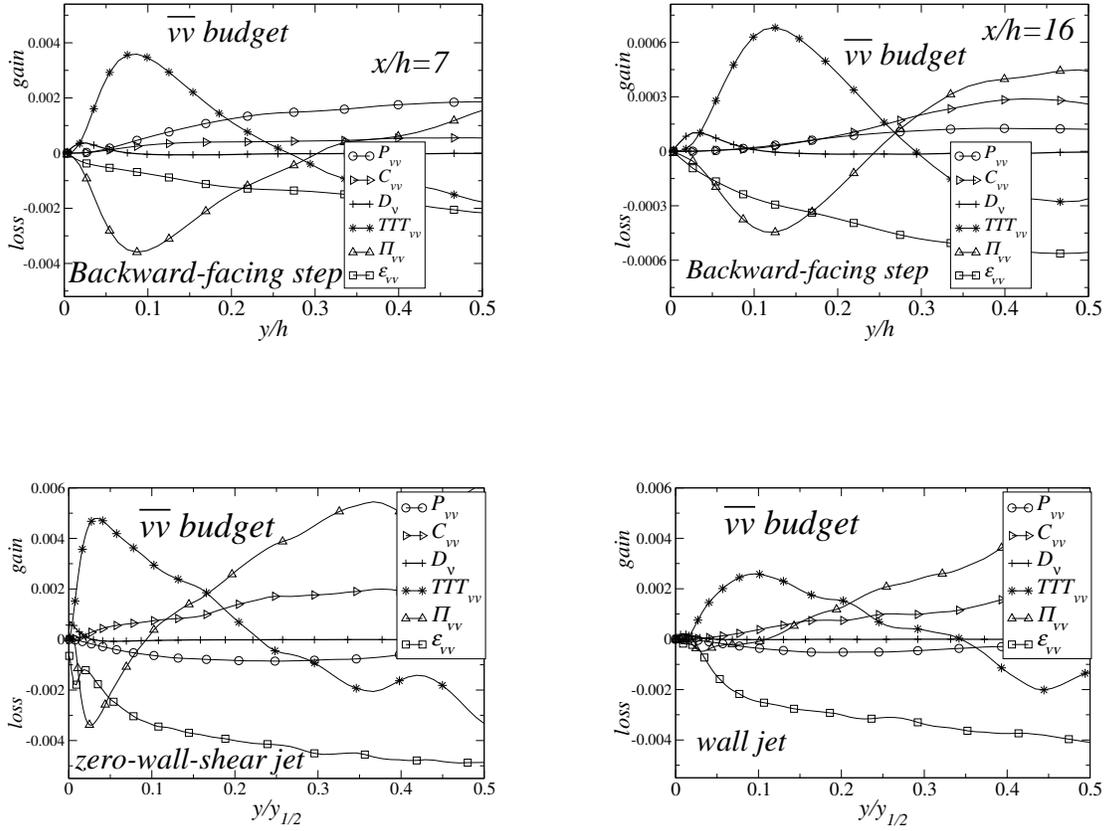
Figure 13: Budgets of the wall-normal stress: see caption of Fig. 11 and Eq.
1
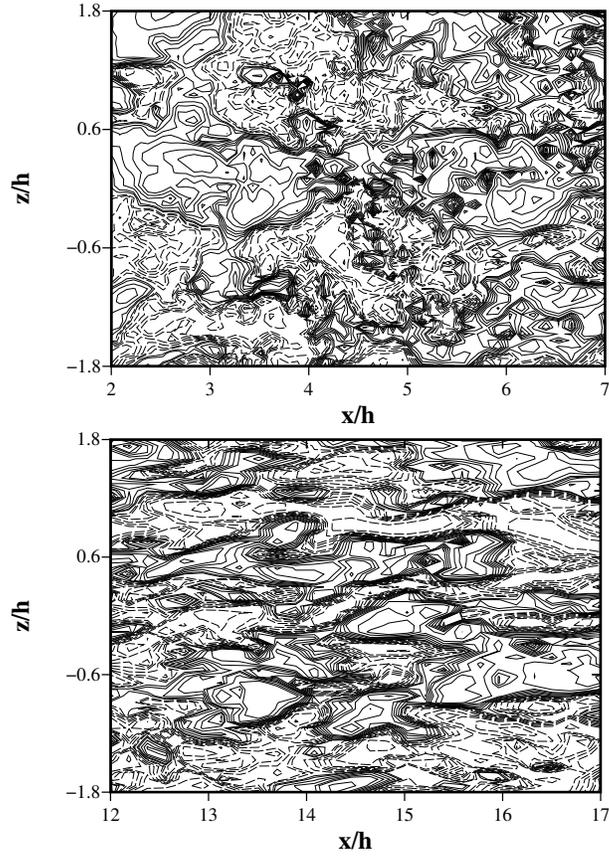
Figure 14: Backward-facing step: contours of instantaneous streamwise veloc-
ity fluctuations, u/U_o, parallel to the wall at $y/h \sim 0.007$. The plot contains
40 contours of u/U_o in the range [-1.5:1.5]. Top: $2 < x/h < 7$. Bottom:
$12 < x/h < 17$
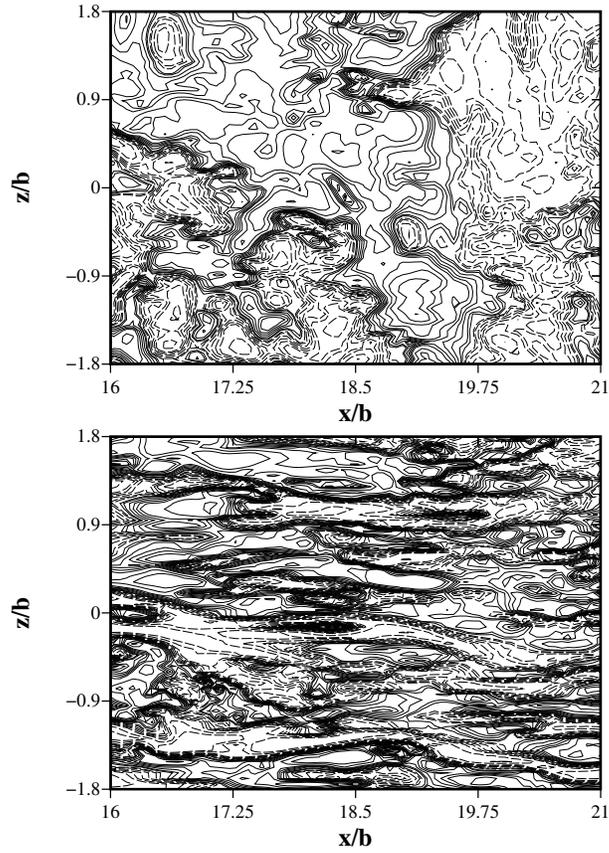
Figure 15: Jet flows: contours of instantaneous streamwise velocity fluctuations, u/U_o, parallel to the wall at $y/y_{1/2} \sim 0.02$. The plot contains 40 contours of u/U_o in the range [-1.5:1.5]. Top: zero-wall-shear jet. Bottom: real wall jet
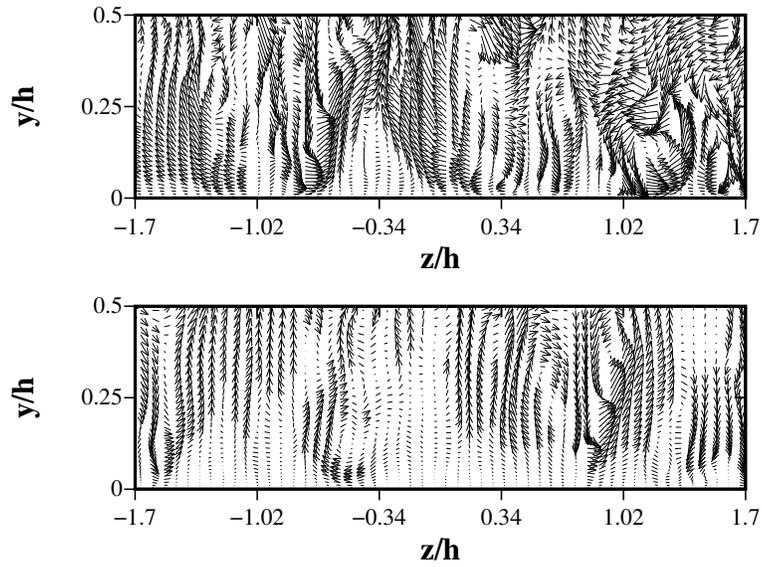
Figure 16: Backward-facing step: instantaneous field of transverse motion $(w/U_o, v/U_o)$ in the cross-flow plane at $x/h = 7$ (top) and $x/h = 15$ (bottom)
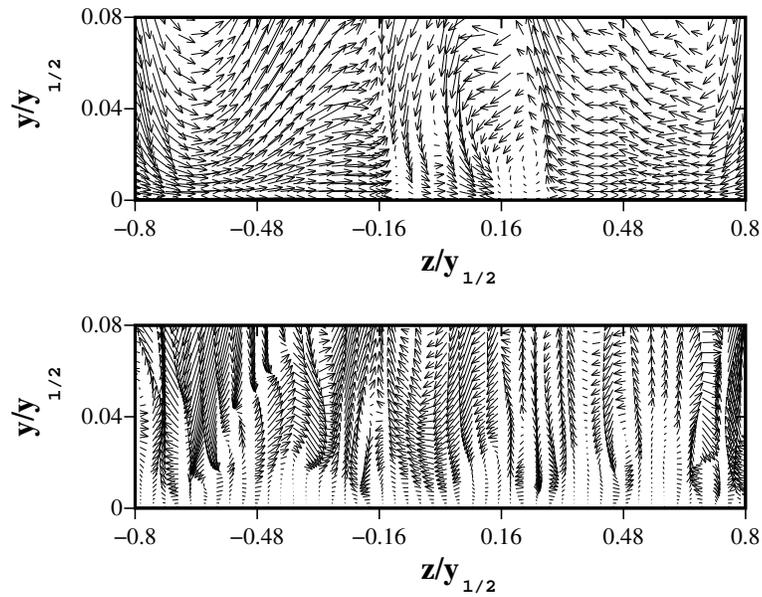
Figure 17: Jet flows: instantaneous field of transverse motion $(w/U_o, v/U_o)$ in the cross-flow plane at $x/b = 20$, zero-wall-shear jet (top), real jet (bottom)
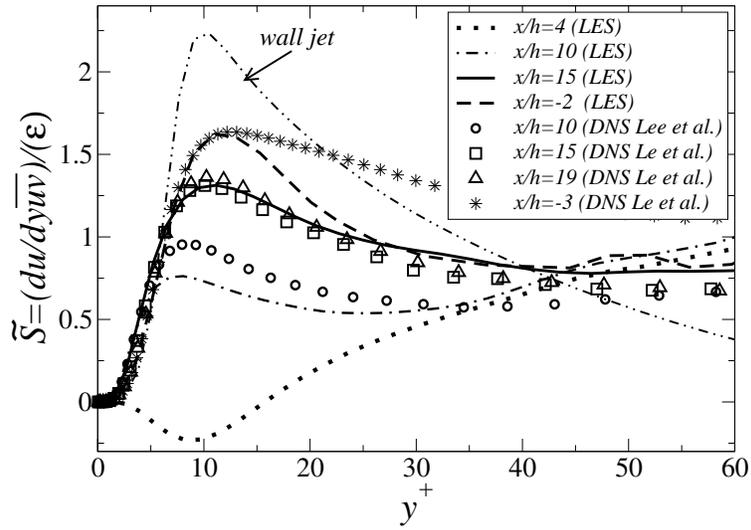
Figure 18: Evolution of the shear parameter, $\tilde{S}$, along the streamwise direction of the backstep flow; comparison with the wall jets
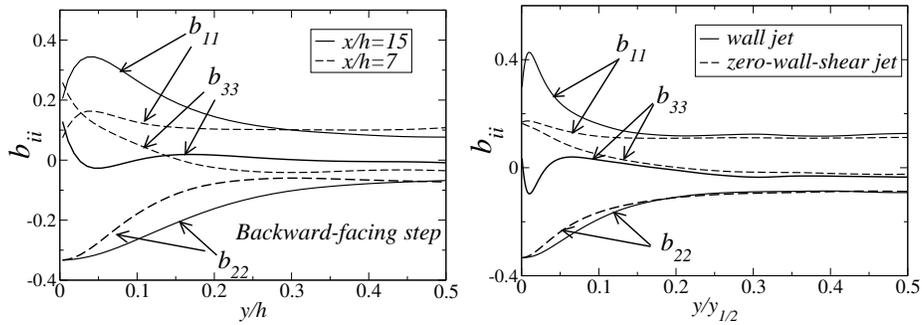
Figure 19: Profiles of the normal-stress anisotropy

42
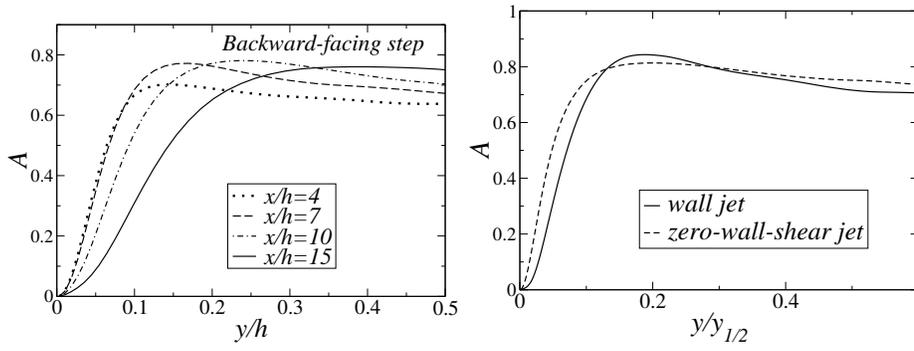
Figure 20: Backward-facing step flow: profiles of the flatness parameter
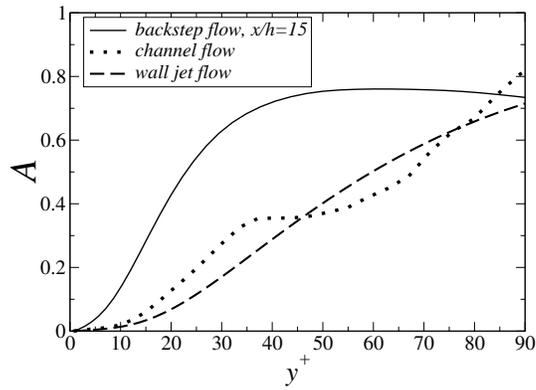
Figure 21: Jet flows: profiles of the flatness parameter
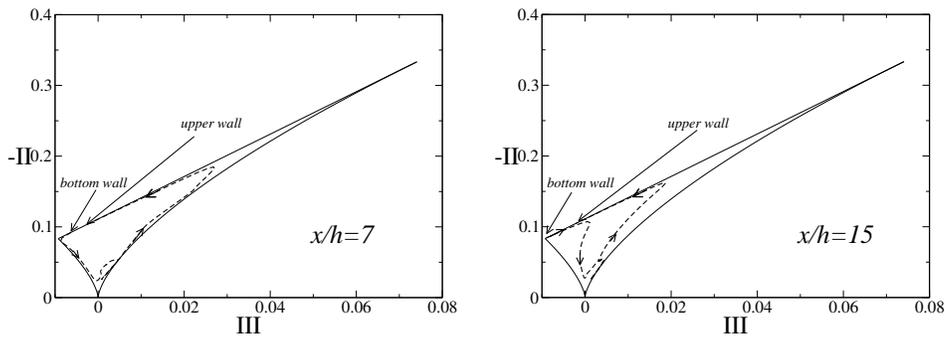
Figure 22: Backward-facing step: anisotropy maps
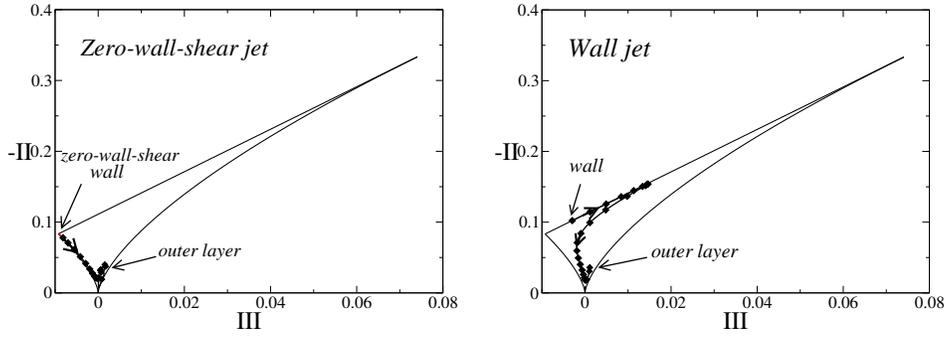
Figure 23: Jet flows: anisotropy maps
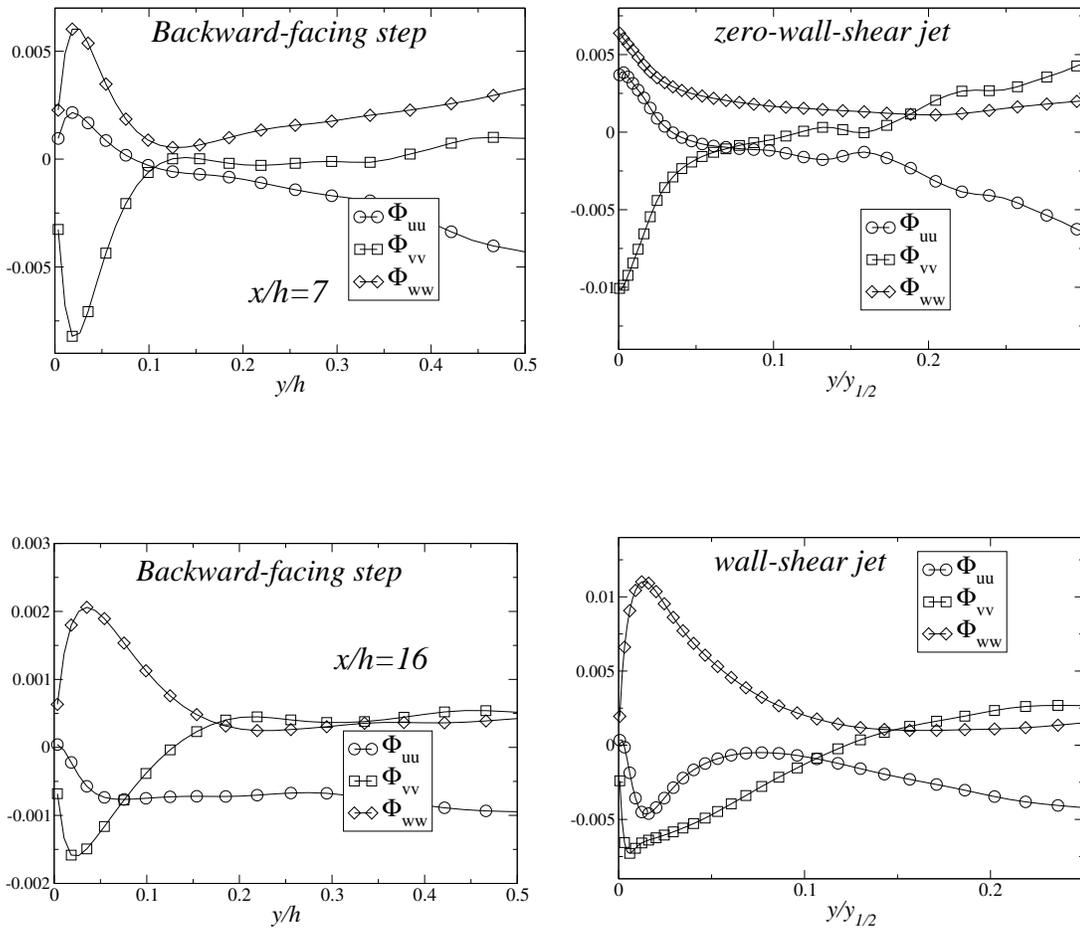
Figure 24: Redistribution of turbulence energy through the pressure-strain term, Φ_{ij}

44
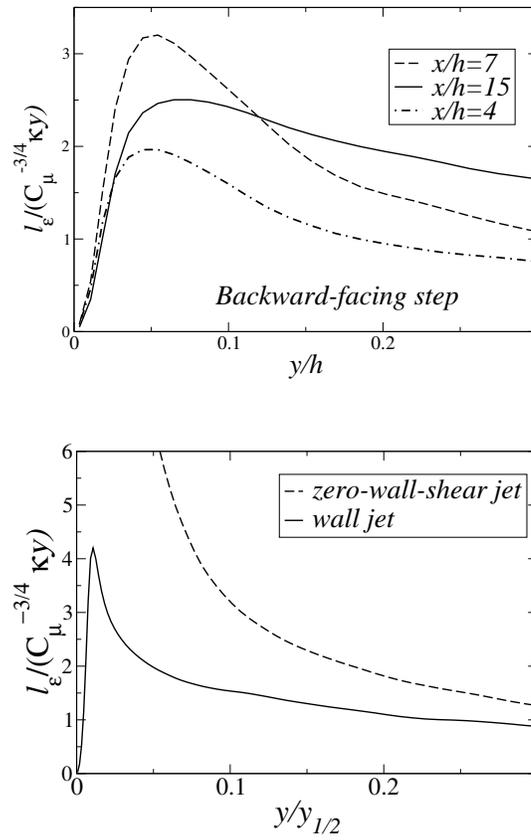
Figure 25: Integral length scale, $l_\varepsilon = k^{3/2}/\varepsilon$, normalised by the equilibrium value
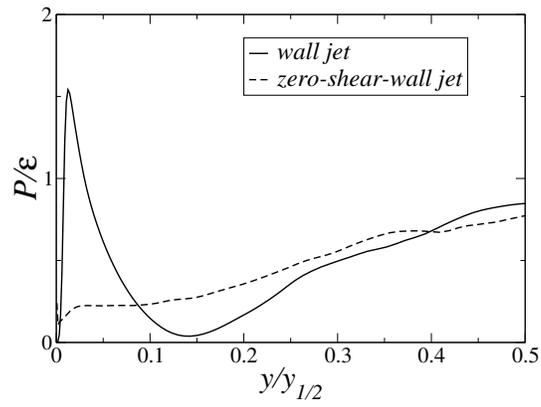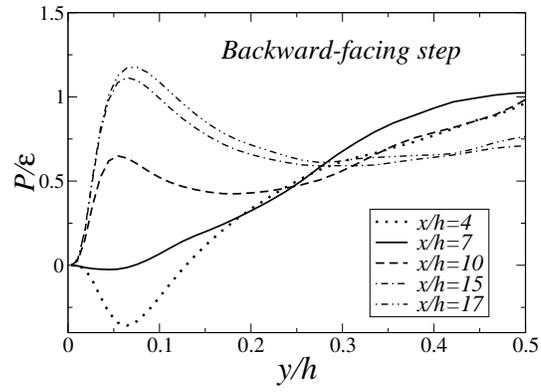
Figure 26: Ratio of production P to dissipation ε of turbulence energy.